

# Bayesian Inference of the Landau Parameter $G'_0$ from Joint Gamow-Teller Measurements

Zidu Lin,<sup>1,2</sup> Gianluca Colò,<sup>3,4</sup> Andrew W. Steiner,<sup>1,5</sup> and Amber Stinson<sup>1</sup>

<sup>1</sup>*Department of Physics and Astronomy, University of Tennessee Knoxville, Knoxville, TN 37996-1200, USA.*

<sup>2</sup>*Department of Physics and Astronomy, University of New Hampshire, Durham, NH 03824, USA.*

<sup>3</sup>*Dipartimento di Fisica, Università degli Studi di Milano, via Celoria 16, 20133 Milano, Italy,*

<sup>4</sup>*INFN, Sezione di Milano, via Celoria 16, 20133 Milano, Italy*

<sup>5</sup>*Physics Division, Oak Ridge National Laboratory, TN 37831, USA.*

The Landau-Migdal parameter  $G'_0$  characterizes the main part of the spin-isospin nucleon-nucleon interaction. Consequently, the  $G'_0$  is closely related to the Gamow-Teller resonance (GTR), the beta and double-beta decay rates of finite nuclei, the spin response of hot and dense nucleonic matter that determines the neutrino-nucleon reaction rates in core-collapse supernovae (CCSNe) and binary neutron star (BNS) mergers, and finally the critical density for pion condensation in neutron stars. Historically, the  $G'_0$  was obtained by fitting the peak location of experimental GTR spectra by using phenomenological pion exchange models, without strict uncertainty quantification. In this letter, for the first time, we report the Bayesian inference of  $G'_0$  by using a self-consistent Skyrme Quasiparticle Random Phase Approximation (QRPA) model and joint constraints from experimental GTR measurements on  $^{208}\text{Pb}$ ,  $^{132}\text{Sn}$ ,  $^{90}\text{Zr}$ . Our extracted  $G'_0$  is  $0.48 \pm 0.034$ , which is close to the prediction of a few existing Skyrme models that consider the spin-isospin observables but is smaller than the extracted ones from pion-exchange models. We hint to possible reasons for this deviation, like the value of the nucleon effective mass  $\frac{m^*}{m}$ . Finally, we demonstrate the influence of  $G'_0$  on neutrino opacities in CCSNe and BNS mergers. The new Skyrme parameterizations from our Bayesian study may also be used to study other spin-isospin-dependent phenomena.

**Introduction.** Understanding the interactions between nucleons is one of the ultimate goals in nuclear physics. The isospin-dependent part of the nuclear force is important for the structure of neutron-rich nuclei, the properties of isospin-symmetric matter, and the evolution and structure of neutron stars. The spin-isospin part of the nuclear force, on the other hand, is crucial for understanding the Gamow-Teller resonance (GTR) in nuclei [1–3] and other charge-exchange (CE) nuclear reactions [4]. Thus, neutrino interactions with dense matter in core-collapse supernovae and neutron star mergers [5–7], beta-decay and neutrinoless double beta-decay rates in finite nuclei [2, 8–10], and pion condensation in dense matter are all related to the spin-isospin part of the nuclear force [11, 12]. The spin-isospin-dependent nuclear force is characterized by the Landau parameter  $G'_0$  [13], and is usually a repulsive force at densities relevant to nuclei and dense matter in massive stars. Although different models were used to extract  $G'_0$ , the extracted values can be compared with each other.

Historically,  $G'_0$  was extracted by fitting it to the peak location of the experimental Gamow-Teller resonance (GTR), assuming experimental or Woods-Saxon single-particle states and either a simplified version of linear response theory or RPA [14–17]. The main limitation of these works is that  $G'_0$  and the single-particle states come from different assumptions, without an underlying microscopic model. In other words, within this scheme, self-consistency is broken. This is an obstacle if extrapolations to other densities or nuclei beyond the reach of terrestrial experiments are envisioned. A further assumption made in most of the published works is that  $G'_0$  is density-independent, whereas in microscopic theories three-body effects naturally imply a density dependence.

To extract  $G'_0$ , often models based on pion exchange (or  $\pi + \rho$ -exchange) have been employed. Note that in these

models, the extracted dimensionless  $g'_0$  is not the commonly defined Landau Migdal parameter  $G'_0$ , but their relationship is  $\frac{m}{m^*} G'_0 \cdot 150 \text{ MeV fm}^3 = g'_0 \cdot 392 \text{ MeV fm}^3$  [1, 15, 18, 19]. We discuss different definitions of this Fermi liquid parameter in the supplemental material. Also note that several crucial assumptions are often made in addition to what is already mentioned. For example, in [15], to extract  $G'_0$ , in the matrix elements the quantity  $\rho_n(r) - \rho_p(r)$  is approximated by a constant  $(N - Z)n_0\gamma/A$ , where  $n_0$  is the saturation density and  $\gamma$  is the so-called attenuation factor, and the effective nucleon mass  $\frac{m^*}{m}$  is assumed to be  $\approx 0.8$ . All these uncontrolled approximations make it difficult to extract a reliable uncertainty on  $G'_0$ .

Although  $G'_0$  characterizes the important spin-isospin-dependent nucleon force that is relevant to many nuclear and astrophysical phenomena, a strict constraint of  $G'_0$  based on joint Gamow-Teller experiments is absent. In this work, for the first time, we use Bayesian inference to infer the value of  $G'_0$ , based on a self-consistent Skyrme QRPA model and joint experimental GTR spectrum measurements.

**Methods.** We first briefly introduce the self-consistent quasi-particle random phase approximation (QRPA) model used in this work. The QRPA calculations were performed on the basis of a Hartree-Fock-Bardeen-Cooper-Schrieffer (HF-BCS) scheme using Skyrme interactions. Given the quasi-particle states, one can build the QRPA matrix equation:

$$\begin{pmatrix} A & B \\ -B^* & -A^* \end{pmatrix} \begin{pmatrix} X^n \\ Y^n \end{pmatrix} = E_n \begin{pmatrix} X^n \\ Y^n \end{pmatrix}, \quad (1)$$

where the detailed expression of the QRPA matrix elements are introduced in [20, 21]. The  $X^n$  and  $Y^n$  are the amplitudes of the quasi-particle configurations that contribute to the eigenstate wave functions. After solving the QRPA matrix equation, the Gamow-Teller strength function is obtained

from the eigenstates, labelled by  $n$ , as

$$S(E) = \sum_n |\langle n | \hat{O}_{\text{GT}} | 0 \rangle|^2 \delta(E - E_n), \quad (2)$$

where  $\hat{O}_{\text{GT}}^\pm = \sum_{i=1}^A \sigma_\pm^i \tau_\pm^i$ . The density-dependent Landau-Migdal parameter  $G'_0(n)$ , is included in the QRPA matrix elements  $A$  and  $B$ . In the present case, we treat only magic nuclei and QRPA reduces to RPA as the superfluid terms vanish.

We use Bayesian inference to obtain constraints on  $G'_0$ . The posterior distribution of Skyrme parameterizations are found by:

$$P_{\text{post}}(\{p\}) = \int \mathcal{L}(\{p\}) P_{\text{prior}}(\{p\}) d\{p\}, \quad (3)$$

where  $\{p\}$  is the set of Skyrme parameters and  $\mathcal{L}(\{p\})$  is the likelihood constraining the parameter distribution of our model. Given  $P_{\text{post}}(\{p\})$ , we can find the posterior distribution of  $G'_0$  as a function of Skyrme parameters. Note that if we ignore the theoretical systematic uncertainty, the likelihood  $\mathcal{L}(\{p\})$  can be written as:

$$\mathcal{L}(\{p\}) = \prod_k \exp \left\{ -\frac{[O_k^{\text{Th}}(\{p\}) - O_k]^2}{2\sigma_k^2} \right\}, \quad (4)$$

where  $O_k^{\text{Th}}$  is the theoretical prediction of the observable  $O_k$  and  $\sigma_k$  is the experimental uncertainty of  $O_k$ .

However, in many cases, the systematic uncertainty coming from theoretical calculations can be obviously larger than experimental measurements (e.g. in the case of calculating the nuclei binding energy and charge radii). Consequently, in this work we consider the unknown systematic theoretical uncertainties in the likelihood by using [22]:

$$\begin{aligned} \mathcal{L}(\{p\}) = & \prod_k \frac{1}{N_k} \int_a^b \exp \left\{ -\frac{[O_k^{\text{Th}}(\{p\}) - \hat{O}_k]^2}{2\sigma_{k,sys}^2} \right\} \\ & \cdot \exp \left\{ -\frac{[O_k - \hat{O}_k]^2}{2\sigma_k^2} \right\} d\hat{O}_k, \end{aligned} \quad (5)$$

where  $\hat{O}_k$  is the ‘‘probabilistic’’ output from the theory that predicts the observable with the mean  $O_k^{\text{Th}}$  and with the uncertainties  $\sigma_{k,sys}$ . Consequently,  $\hat{O}_k$  can deviate from  $O_k^{\text{Th}}$  due to the theoretical uncertainty. Also note that in Eq. (5) the normalization factors  $N_k$  cannot be ignored since they are an implicit function of  $\sigma_{k,sys}$ . Besides ground state properties of finite nuclei, in this letter we include GTR measurements in the Bayesian inference. The full list of Bayesian constraints are described in the supplemental material.

The Skyrme parameterizations sampled from GTR posterior are then used to calculate many-body corrections on charged-current neutrino opacity, which play important roles in understanding the explosion mechanism of core-collapse supernovae (CCSNe) and the formation of heavy elements

in both CCSNe and binary neutron star (BNS) mergers [5–7, 23–25]. To quantify the effect of many-body corrections on charged current neutrino-nucleon reactions, we define:

$$\text{MB}_{ax}^{(\nu_e/\bar{\nu}_e, e^-/e^+)} = \frac{\int \frac{1}{V} \frac{d^2 \sigma_{ax}^\pm}{d\cos\theta dE_{e^-/e^+}} d\cos\theta dE_{e^-/e^+}}{\int \frac{1}{V} \frac{d^2 \sigma_{0,ax}^\pm}{d\cos\theta} d\cos\theta}, \quad (6)$$

where the integrand of the numerator is the axial-current part of the differential cross section including many-body corrections:

$$\begin{aligned} \frac{1}{V} \frac{d^2 \sigma_{ax}^\pm}{d\cos\theta dE_{e^-/e^+}} = & \frac{G_F^2 g_A^2 p_{e^-/e^+} E_{e^-/e^+}}{4\pi^2} \\ & \times (3 - \cos\theta) S_A(q_0, q). \end{aligned} \quad (7)$$

The  $g_A \approx 1.23$ . The many-body correction on axial-current neutrino-nucleon corrections is encoded in  $S_A(q_0, q)$  which is sensitive to the strength of  $G'_0$  (its derivation is provided in the supplemental material). The  $q_0$  and  $q$  are transferred neutrino energy and momentum. The integrand of the denominator is the free-space differential inverse mean free path  $V^{-1} d\sigma_0^\pm/d\cos\theta$  defined similarly as Eq. (7), but with the correction  $S_A(q_0, q)$  replaced by  $2\pi n$ , where  $n$  is the number density of neutrons (protons) for electron neutrino (anti-electron neutrino) reactions. The importance of nucleon-nucleon residual interaction in determining the neutrino-nucleon interactions has been discussed in [6, 23], and only recently the correlation between  $G'_0$  and the many-body corrections on axial charged current neutrino-nucleon reactions was systematically studied [25]. Comparing to Ref. [25], in this letter we improve the calculation of neutrino-nucleon many-body corrections by strictly solving the Bethe-Salpeter equation based on the method proposed in Ref. [26, 27].

**Results.** The GT spectra is characterized by the location of its main peak ( $E_{\text{GT}}$ ) and by the percentage of strength exhausted in GT region, denoted as  $m_0\%$  in the following. Historically, the  $G'_0$  was extracted based on phenomenological models and by fitting  $E_{\text{GT}}$ . However, the extracted values of  $G'_0$  are not consistent (e.g.  $G'_0 = 1.020$  ( $^{48}\text{Ca}$ ),  $G'_0 = 1.24$  ( $^{90}\text{Zr}$ ) and  $G'_0 = 1.50$  ( $^{208}\text{Pb}$ ) from Ref. [15];  $G'_0 = 1.10$  ( $^{90}\text{Zr}$ ) and  $G'_0 = 1.17$  ( $^{208}\text{Pb}$ ) from Ref. [41, 42];  $G'_0 = 1.24$  ( $^{132}\text{Sn}$ ) from Ref. [43]). Here, we perform Bayesian inference including constraints of  $E_{\text{GT}}$  and  $m_0\%$  from  $^{208}\text{Pb}$ ,  $^{132}\text{Sn}$ ,  $^{90}\text{Zr}$  (denoted as GTall constraints) and investigate the dependence of GT spectra features on  $G'_0$  in a self-consistent QPRA model. We also perform four additional Bayesian inference with only GTR constraints from  $^{208}\text{Pb}$  (GTPb),  $^{132}\text{Sn}$  (GTSn),  $^{90}\text{Zr}$  (GTZr), and without any GTR constraints (noGT).

In Fig. 1, we show the distributions of  $(m_0\%, G'_0)$  sampled from Bayesian posteriors, and compare it with existing Skyrme models. The correlation between  $G'_0$  and  $m_0\%$  is observed both in the existing Skyrme models (black squares) and in the posterior without constraints of  $E_{\text{GT}}$  and  $m_0\%$  (colored scattering dots). The posterior (black contours) of GTall shows the pinned-down area favored by GTR measurements. We observe that the correlation between  $G'_0$  and  $m_0\%$  in  $^{90}\text{Zr}$

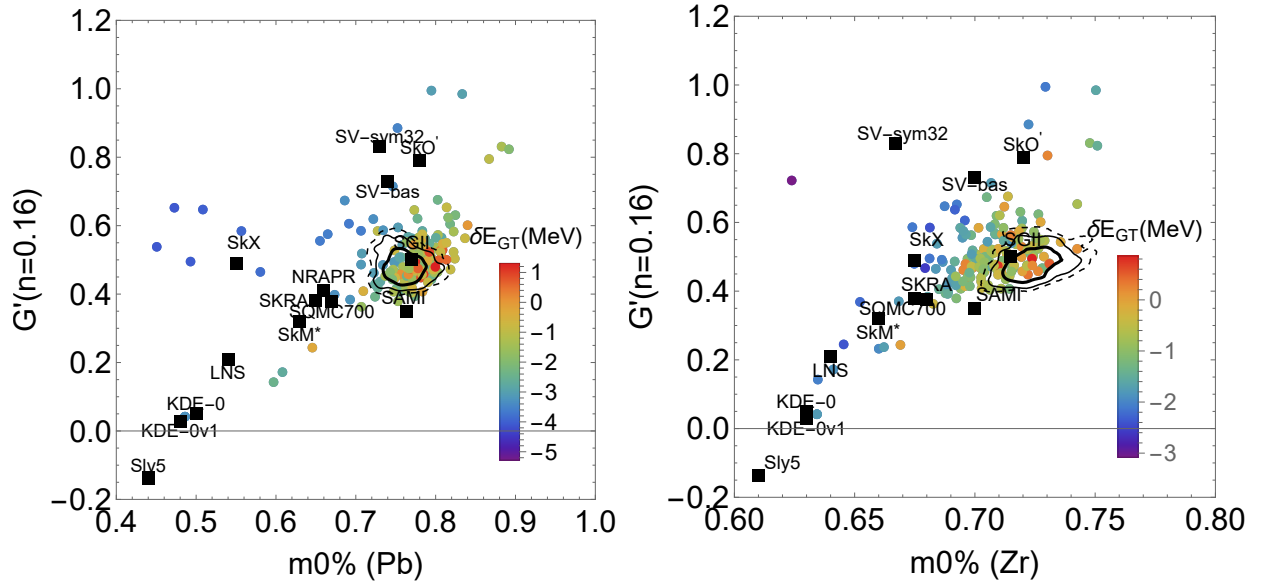


FIG. 1. The distribution of  $G'_0$ ,  $m_0\%$  and  $\delta E_{GT}$  in GTall and noGT simulation, where the latter is defined as  $\delta E_{GT} = E_{GT}^{model} - E_{GT}^{exp}$ . The left panel shows the  $G'_0$  dependence on  $m_0\%$  of  $^{208}\text{Pb}$ . The right panel shows the  $G'_0$  dependence on  $m_0\%$  of  $^{90}\text{Zr}$ . The colored scattered points are sampled from the Bayesian posterior distribution without Gamow-Teller constraints (noGT). The black solid thick, thin, dashed contours represent the 68%, 95%, and 99% confidence interval of a posterior distribution including all Gamow-Teller constraints (GTall). The distribution of  $G'_0$  vs  $m_0\%$  in  $^{132}\text{Sn}$  behaves similarly as the one in  $^{208}\text{Pb}$ , so it is not shown in the manuscript. The squares represent 15 Skyrme models (SLy4 [28], SLy5 [28], SV-bas [29], KDE0 [30], SAMI [31], SkX [32], SkM\* [33], SkO' [34], SV-sym32 [29], SGII [35], KDE0v1 [30], LNS [36], NRAPR [37], SKRA [38], SQMC700 [39]). Note that NPAPR predicts  $E_{GT}$  of  $^{90}\text{Zr}$  equals to 11.3 MeV which is significantly lower than the measurement and is lying beyond the scope of the left panel.

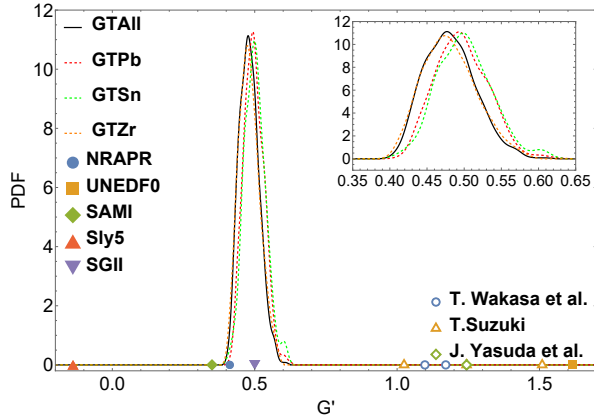


FIG. 2. The posterior distribution of  $G'_0$ . The red dashed, green dashed, orange dashed, and black dashed curves are the posterior of  $G'_0$  extracted from Bayesian inferences with constraints of only  $^{208}\text{Pb}$  (GTPb), only  $^{132}\text{Sn}$  (GTSn), only  $^{90}\text{Zr}$  (GTZr), and noGT, respectively. The black solid curve represents the posterior of  $G'_0$  from a Bayesian inference including all the aforementioned GTR measurements (GTall). The sub panel in the corner show the zoom-in feature of  $G'_0$  distributions. The filled colored points represent the  $G'_0$  of existing Skyrme models (NRAPR [37], UNEDF0 [40], SAMI [31], Sly5 [28], SGII [35]) and the hollow colored points represent the extracted  $G'_0$  based on phenomenological pion-exchange models (T. Wakasa et al. [41, 42], T. Suzuki [15], J. Yasuda et al. [43]). A brief discussion on the difference between the extracted  $G'_0$  is given in supplemental material.

is stronger than that in  $^{208}\text{Pb}$  and  $^{132}\text{Sn}$ . Another interesting feature is that at fixed  $m_0\%$  the  $G'_0$  tends to increase as the deviation between Skyrme and experimental  $E_{GT}$  increases. We then compare the sampled data points from the Bayesian posterior with existing Skyrme models.

However, the correlation between  $G'_0$  and  $E_{GT}$  is not strong in our Bayesian inference, which is also observed in Ref. [54]. The weakening of this correlation may be due to the fact that a specific value of  $E_{GT}$  may correspond to different values of  $G'_0$  given the uncertainty of spin-orbit splitting, causing a degeneracy problem. This issue is discussed in the supplemental material. We also provide the quantified Pearson correlation among the GTR quantities, and ground state quantities from various nuclei in the supplemental material.

In Fig. 2, based on the posterior of  $G'_0$  constrained by joint GTR measurements (the black solid curve), we conclude that  $G'_0 = 0.48 \pm 0.034$ . The posteriors of  $G'_0$  of GTPb (red dashed), GTSn (green dashed), and GTZr (orange dashed), largely overlaps with the GTall.

We further compare the posterior distributions of the  $G'_0$  with those predicted by existing Skyrme models (colored filled points), which are poorly constrained and have no uncertainty quantification. Many successful Skyrme models giving good ground state nuclei properties [55] fail to reproduce GTR features, and only a few (e.g. SGII, SAMI) predict features close to the posterior constrained by joint GTR experiments. We also observe that the extracted  $G'_0$  based on pion-exchange models (hollow colored points) are larger than the

		Experiment	nuSkyI	nuSkyII	nuSkyIII	
<sup>208</sup> Pb	$B/A$ [MeV]	7.87 [44, 45]	7.73	7.89	7.89	
	$R_{ch}$ [fm]	5.50 [44, 45]	5.47	5.44	5.44	
	$F_{ch}$ []	0.409 [46]	0.412	0.418	0.417	
	$\Delta F$ []	0.041±0.013 [46]	0.0241	0.0185	0.0288	
	$E_{\text{GT}}$ [MeV]	19.2 [47, 48]	20.04	20.05	19.46	
	$m_0\%$ []	74% ± 1.48% [47, 48]	75.6%	77.0%	74.8%	
<sup>132</sup> Sn	$B/A$ [MeV]	8.355 [44, 45]	8.25	8.36	8.37	
	$R_{ch}$ [fm]	4.71 [44, 45]	4.69	4.67	4.67	
	$E_{\text{GT}}$ [MeV]	13.97 [43]	14.66	14.56	13.97	
	$m_0\%$ []	81% ± 16% [43]	79.23%	79.54%	78.72%	
<sup>90</sup> Zr	$B/A$ [MeV]	8.71 [44, 45]	8.65	8.74	8.79	
	$R_{ch}$ [fm]	4.27 [44, 45]	4.23	4.23	4.22	
	$E_{\text{GT}}$ [MeV]	15.8 [49]	16.2	16.0	16.15	
	$m_0\%$ []	68% ± 1.4% [49]	69.8%	72.8%	70.7%	
<sup>48</sup> Ca	$B/A$ [MeV]	8.67 [44, 45]	8.78	8.82	8.86	
	$R_{ch}$ [fm]	3.48 [44, 45]	3.46	3.48	3.46	
	$F_{ch}$ []	0.158 [50]	0.155	0.154	0.155	
	$\Delta F$ []	0.0277±0.0055 [50]	0.0423	0.036	0.0422	
	$E_{\text{GT}}$ [MeV]	10.5 [51]	11.0	10.6	10.8	
Landau-Migdal Parameter		$G'_0$ []	0.44 ± 0.09 (this work)	0.35	0.44	0.41
NS	$R_{1.4}$ [km]	12.71 <sup>+1.14</sup> <sub>-1.19</sub> [52] ; 13.02 <sup>+1.24</sup> <sub>-1.06</sub> [53]	12.12	N/A	12.20	
	$M_{max}$ [ $M_\odot$ ]	> 2.0	2.08	N/A	2.05	

TABLE I. The basic properties of nuclei and neutron stars predicted by the new Skyrme sets nuSky. In this Table,  $\Delta F$  is the difference between the weak and charge form factors  $F_w$  and  $F_{ch}$ . The fraction of GT strength  $m\%$  is defined as the ratio of the area covered by the GTR spectrum in the intervals [15, 24], [9, 24] and [12, 22] MeV to the area covered by the spectrum below 31 MeV, for <sup>208</sup>Pb, <sup>132</sup>Sn and <sup>90</sup>Zr GTR spectrum respectively. The relative uncertainty of accurately measured values (the binding energy, the charge radii and the peak location of GTR of finite nuclei) are artificially chosen to be 2% of the experimental values to ensure the feasibility of Monte Carlo simulations. A full table that summarizes all the Bayesian constraints applied in this work is provided in the supplemental material.

Skyrme posterior. The possible reason for this difference is discussed in supplemental material.

We propose three new Skyrme sets (nuSkyI, nuSkyII and nuSkyIII) found in the Bayesian inference of GTall, which reasonably describe both the ground state and Gamow-Teller resonance properties of various finite nuclei. The nuSkyI and nuSkyIII also give reasonable basic neutron star properties as summarized in Tab. I. The symmetry energy slope of nuSkyI, nuSkyII and nuSkyIII is  $L = 53.4$  MeV,  $L = 19.7$  MeV and  $L = 64.2$  MeV respectively. Note that the  $L$  corresponding to nuSkyII is too small to support a  $2.0 M_\odot$  neutron star and is not suitable for describing massive star properties. This new Skyrme parameterization series (nuSky) may provide a self-consistent description of the macroscopic massive star properties (such as the neutron star mass and radii) and the microscopic weak interaction properties in the stars (such as neutrino-nucleon and neutrino-nucleus interactions in hot and dense matter). The posterior distributions of the properties of finite-nuclei ground state and excited states are summarized in the supplemental material.

In Fig. 3, we present the statistical distribution of  $MB_{ax}$  based on the posterior constrained by joint GTR measurements (colored points), and compare it with those based on

existing Skyrme parameterizations (black squares). The distribution based on existing Skyrme models and the study in Ref. [25] indicate that  $MB_{ax}^{(\nu_e, e^-)}$  ( $MB_{ax}^{(\bar{\nu}_e, e^+)}$ ) decreases (increases) with the increase of  $G'_0$ . For the first time, by applying GTR constraints we significantly reduce the uncertainty of  $MB_{ax}$  due to variation of  $G'_0$ . The remaining uncertainty of  $MB_{ax}$  mainly comes from the variation of  $\delta U = U_n - U_p$  at sub-saturation densities and results in a wide spreading of  $MB_{ax}$  along the vertical axis. The neutron skin measurements [46, 50] applied in our Bayesian inference cannot tightly constrain the symmetry energy and  $\delta U$  at sub-saturation densities. In the future, stronger constraints on the density-dependent symmetry energy slope and the constraints on  $G'_0$  should be applied together to pin down the neutrino opacity at subsaturation densities.

**Summary.** The nonrelativistic Skyrme EDF is one of the few models that can self-consistently describe both the ground state properties and the charge-exchange processes of finite nuclei. Within the Skyrme framework, systematic calculations of the GT strength and Bayesian inferences are possible while this would be otherwise too challenging.

For the first time, we use Bayesian inference to obtain the probability distribution of  $G'_0$ . The GT spectra are calculated

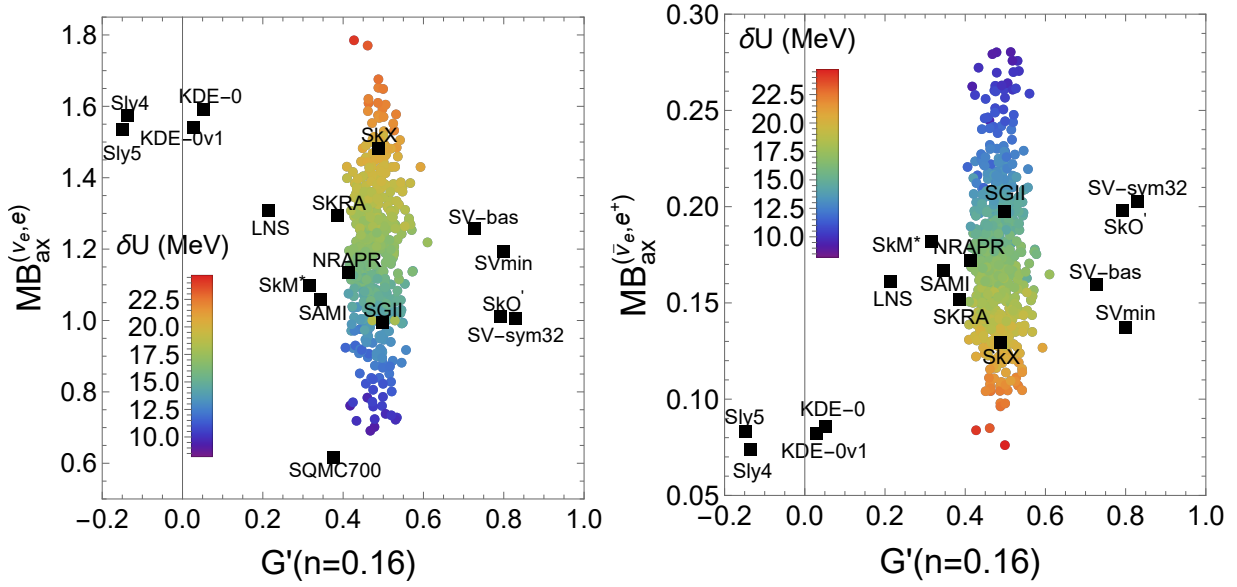


FIG. 3. The dependence of neutrino-nucleon many-body (MB) corrections (defined in Eq. 6) on  $G'_0$  from the GTall calculation described in the text. The black squares represent the MB corrections based on existing models. The left panel shows the dependence of many-body correction of  $\nu_e(n, p)e^-$  on  $G'_0$  and the right panel shows the dependence of many-body correction of  $\bar{\nu}_e(p, n)e^+$  on  $G'_0$ . The color represents the difference of nucleon potentials  $\delta U = U_n - U_p$ , which is another factor determining the many-body corrections. The  $\nu_e(n, p)e^-$ ,  $\bar{\nu}_e(p, n)e^+$  reactions and the  $\delta U$  examined here are calculated at  $n=0.02 \text{ fm}^{-3}$ ,  $T = 10 \text{ MeV}$ , incoming neutrino energy  $E_\nu = 30 \text{ MeV}$  and  $Y_e = 0.05$ .

using self-consistent Skyrme QRPA and the GT experiments are used jointly to constrain the models. The ground-state properties and spin-orbit splitting values of several representative closed-shell nuclei are also employed to constrain the models. From the posterior distribution, the value of  $G'_0$  with quantified uncertainty is  $0.48 \pm 0.034$ . This value is close to that predicted only by a limited set of Skyrme models. Moreover, it is smaller than the  $G'_0$  values reported in previous work and based on pion exchange models. We should consider that in these models empirical single-particle states are generally input, whereas ours is a self-consistent model. The effective nucleon mass is certainly different in the two cases. This warns against the use of hybrid Hartree Fock + RPA models (which use Skyrme parameterization to calculate the mean field and empirically fitted values of  $G'_0$  to calculate the RPA residual force) to estimate neutrino-dense matter reactions [23]. In addition, we quantitatively study the correlations among the excited state GTR properties and the ground state properties on various nuclei.

We propose a small series of three new Skyrme sets, named nuSky\*, that are obtained from the Bayesian posterior distributions. The difference between these three sets is described in the supplemental material. These new Skyrme parameterizations may be used to predict the GTR spectrum of other nuclei and the neutrino-nucleus interactions. The full dataset of our Bayesian inference (available in 10.5281/zenodo.15537195) can be used as training data for constructing emulators of future GTR calculations, and can also be used to search for optimized Skyrme models that satisfy both nuclear matter and GTR constraints. Additionally, the extracted

$G'_0$  with quantified uncertainties has been used for constraining the calculations of charged current neutrino-nucleon interactions in the dense nucleonic matter of CCSNe and BNS mergers.

In the future, application of nuSky models to study charged current neutrino reactions may yield more insights to macroscopic star and microscopic weak interaction properties. It may also be necessary to invent fast and accurate emulators of GTR features to improve the quality of Bayesian inference.

### Acknowledgements

ZL and AWS were supported by NSF PHY 21-16686. AWS was also supported by the Department of Energy Office of Nuclear Physics. This work used Bridges2 at University of Pittsburgh through allocation PHY230061 from the Advanced Cyberinfrastructure Coordination Ecosystem: Services & Support (ACCESS) program, which is supported by U.S. National Science Foundation grants #2138259, #2138286, #2138307, #2137603, and #2138296.

- 
- [1] F. Osterfeld, Rev. Mod. Phys. **64**, 491 (1992).
  - [2] T. Suzuki and M. Honma, Phys. Rev. C **87**, 014607 (2013), 1211.4078.
  - [3] A. Byelikov, T. Adachi, H. Fujita, K. Fujita, Y. Fujita, K. Hatanaka, A. Heger, Y. Kalmykov, K. Kawase, K. Langanke, et al., Phys. Rev. Lett. **98**, 082501 (2007),

- URL <https://link.aps.org/doi/10.1103/PhysRevLett.98.082501>.
- [4] R. G. T. Zegers (Springer Nature Singapore, Singapore, 2023), pp. 739–773, ISBN 978-981-19-6345-2, URL [https://doi.org/10.1007/978-981-19-6345-2\\_77](https://doi.org/10.1007/978-981-19-6345-2_77).
  - [5] S. Reddy, M. Prakash, and J. M. Lattimer, *Phys. Rev. D* **58**, 013009 (1998), astro-ph/9710115.
  - [6] A. Burrows and R. F. Sawyer, *Phys. Rev. C* **58**, 554 (1998), astro-ph/9801082.
  - [7] C. J. Horowitz, O. L. Caballero, Z. Lin, E. O'Connor, and A. Schwenk, *Phys. Rev. C* **95**, 025801 (2017), URL <https://link.aps.org/doi/10.1103/PhysRevC.95.025801>.
  - [8] J. Engel, P. Vogel, and M. R. Zimbauer, *Phys. Rev. C* **37**, 731 (1988), URL <https://link.aps.org/doi/10.1103/PhysRevC.37.731>.
  - [9] Y.-Z. Qian, W. C. Haxton, K. Langanke, and P. Vogel, *Phys. Rev. C* **55**, 1532 (1997), URL <https://link.aps.org/doi/10.1103/PhysRevC.55.1532>.
  - [10] Y. F. Niu, Z. M. Niu, G. Colò, and E. Vigezzi, *Phys. Rev. Lett.* **114**, 142501 (2015), URL <https://link.aps.org/doi/10.1103/PhysRevLett.114.142501>.
  - [11] A. B. Migdal, E. E. Saperstein, M. A. Troitsky, and D. N. Voskresensky, *Phys. Rept.* **192**, 179 (1990).
  - [12] G. Baym and E. Flowers, *Nucl. Phys. A* **222**, 29 (1974).
  - [13] L. D. Landau, *Zh. Eksp. Teor. Fiz.* **30**, 1058 (1956).
  - [14] G. Bertsch, D. Cha, and H. Toki, *Phys. Rev. C* **24**, 533 (1981), URL <https://link.aps.org/doi/10.1103/PhysRevC.24.533>.
  - [15] T. Suzuki, *Nucl. Phys. A* **379**, 110 (1982).
  - [16] K. Nishida and M. Ichimura, *Phys. Rev. C* **51**, 269 (1995), URL <https://link.aps.org/doi/10.1103/PhysRevC.51.269>.
  - [17] T. Wakasa, M. Ichimura, and H. Sakai, *Phys. Rev. C* **72**, 067303 (2005), URL <https://link.aps.org/doi/10.1103/PhysRevC.72.067303>.
  - [18] M. Bender, J. Dobaczewski, J. Engel, and W. Nazarewicz, *Phys. Rev. C* **65**, 054322 (2002), nucl-th/0112056.
  - [19] I. S. Towner, *Phys. Rept.* **155**, 263 (1987).
  - [20] S. Fracasso and G. Colo, *Phys. Rev. C* **76**, 044307 (2007), 0704.2892.
  - [21] S. Fracasso and G. Colò, *Phys. Rev. C* **72**, 064310 (2005), URL <https://link.aps.org/doi/10.1103/PhysRevC.72.064310>.
  - [22] M. Al-Mamun, A. W. Steiner, J. Nättilä, J. Lange, R. O'Shaughnessy, I. Tews, S. Gandolfi, C. Heinke, and S. Han, *Phys. Rev. Lett.* **126**, 061101 (2021), 2008.12817.
  - [23] S. Reddy, M. Prakash, J. M. Lattimer, and J. A. Pons, *Phys. Rev. C* **59**, 2888 (1999), URL <https://link.aps.org/doi/10.1103/PhysRevC.59.2888>.
  - [24] Y.-Z. Ma, Z. Lin, B.-N. Lu, S. Elhatisari, D. Lee, N. Li, U.-G. Meißner, A. W. Steiner, and Q. Wang, *Phys. Rev. Lett.* **132**, 232502 (2024), URL <https://link.aps.org/doi/10.1103/PhysRevLett.132.232502>.
  - [25] Z. Lin, A. W. Steiner, and J. Margueron, *Phys. Rev. C* **107**, 015804 (2023), URL <https://link.aps.org/doi/10.1103/PhysRevC.107.015804>.
  - [26] E. S. Hernandez, J. Navarro, and A. Polls, *Nucl. Phys. A* **658**, 327 (1999).
  - [27] J. Margueron, J. Navarro, and N. Van Giai, *Phys. Rev. C* **74**, 015805 (2006), nucl-th/0604019.
  - [28] E. Chabanat, P. Bonche, P. Haensel, J. Meyer, and R. Schaeffer, *Nucl. Phys. A* **635**, 231 (1998), [Erratum: *Nucl. Phys. A* **643**, 441–441 (1998)].
  - [29] P. Klüpfel, P.-G. Reinhard, T. J. Bürvenich, and J. A. Maruhn, *Phys. Rev. C* **79**, 034310 (2009), URL <https://link.aps.org/doi/10.1103/PhysRevC.79.034310>.
  - [30] B. K. Agrawal, S. Shlomo, and V. K. Au, *Phys. Rev. C* **72**, 014310 (2005), URL <https://link.aps.org/doi/10.1103/PhysRevC.72.014310>.
  - [31] X. Roca-Maza, G. Colo, and H. Sagawa, *Phys. Rev. C* **86**, 031306 (2012), 1205.3958.
  - [32] B. Alex Brown, *Phys. Rev. C* **58**, 220 (1998), URL <https://link.aps.org/doi/10.1103/PhysRevC.58.220>.
  - [33] J. Bartel, P. Quentin, M. Brack, C. Guet, and H. B. Hakansson, *Nucl. Phys. A* **386**, 79 (1982).
  - [34] P.-G. Reinhard, D. J. Dean, W. Nazarewicz, J. Dobaczewski, J. A. Maruhn, and M. R. Strayer, *Phys. Rev. C* **60**, 014316 (1999), URL <https://link.aps.org/doi/10.1103/PhysRevC.60.014316>.
  - [35] N. van Giai and H. Sagawa, *Phys. Lett. B* **106**, 379 (1981).
  - [36] L. G. Cao, U. Lombardo, C. W. Shen, and N. V. Giai, *Phys. Rev. C* **73**, 014313 (2006), URL <https://link.aps.org/doi/10.1103/PhysRevC.73.014313>.
  - [37] A. W. Steiner, M. Prakash, J. M. Lattimer, and P. J. Ellis, *Phys. Rept.* **411**, 325 (2005), nucl-th/0410066.
  - [38] M. Rashdan, *Modern Physics Letters A* **15**, 1287 (2000).
  - [39] P. A. M. Guichon, H. H. Matevosyan, N. Sandulescu, and A. W. Thomas, *Nucl. Phys. A* **772**, 1 (2006), nucl-th/0603044.
  - [40] M. Kortelainen, T. Lesinski, J. Moré, W. Nazarewicz, J. Sarich, N. Schunck, M. V. Stoitsov, and S. Wild, *Phys. Rev. C* **82**, 024313 (2010), URL <https://link.aps.org/doi/10.1103/PhysRevC.82.024313>.
  - [41] T. Wakasa, M. Ichimura, and H. Sakai, *Phys. Rev. C* **72**, 067303 (2005), nucl-ex/0411055.
  - [42] T. Wakasa et al., *Phys. Rev. C* **85**, 064606 (2012).
  - [43] J. Yasuda, M. Sasano, R. G. T. Zegers, H. Baba, D. Bazin, W. Chao, M. Dozono, N. Fukuda, N. Inabe, T. Isobe, et al., *Phys. Rev. Lett.* **121**, 132501 (2018), URL <https://link.aps.org/doi/10.1103/PhysRevLett.121.132501>.
  - [44] M. Wang, G. Audi, A. H. Wapstra, F. G. Kondev, M. MacCormick, X. Xu, and B. Pfeiffer, *Chin. Phys. C* **36**, 1603 (2012).
  - [45] I. Angeli and K. P. Marinova, *Atom. Data Nucl. Data Tabl.* **99**, 69 (2013).
  - [46] D. Adhikari et al. (PREX), *Phys. Rev. Lett.* **126**, 172502 (2021), 2102.10767.
  - [47] T. Wakasa, M. Okamoto, M. Dozono, K. Hatanaka, M. Ichimura, S. Kuroita, Y. Maeda, H. Miyasako, T. Noro, T. Saito, et al., *Phys. Rev. C* **85**, 064606 (2012), URL <https://link.aps.org/doi/10.1103/PhysRevC.85.064606>.
  - [48] H. Akimune, I. Daito, Y. Fujita, M. Fujiwara, M. B. Greenfield, M. N. Harakeh, T. Inomata, J. Jänecke, K. Katori, S. Nakayama, et al., *Phys. Rev. C* **52**, 604 (1995), URL <https://link.aps.org/doi/10.1103/PhysRevC.52.604>.
  - [49] T. Wakasa, H. Sakai, H. Okamura, H. Otsu, S. Fujita, S. Ishida, N. Sakamoto, T. Uesaka, Y. Satou, M. B. Greenfield, et al., *Phys. Rev. C* **55**, 2909 (1997), URL <https://link.aps.org/doi/10.1103/PhysRevC.55.2909>.
  - [50] D. Adhikari et al. (CREX), *Phys. Rev. Lett.* **129**, 042501 (2022), 2205.11593.
  - [51] K. Yako, M. Sasano, K. Miki, H. Sakai, M. Dozono, D. Frekers, M. B. Greenfield, K. Hatanaka, E. Ihara, M. Kato, et al., *Phys. Rev. Lett.* **103**, 012503 (2009), URL <https://link.aps.org/doi/10.1103/PhysRevLett.103.012503>.
  - [52] T. E. Riley et al., *Astrophys. J. Lett.* **887**, L21 (2019), 1912.05702.

- [53] M. C. Miller et al., *Astrophys. J. Lett.* **887**, L24 (2019), 1912.05705.
- [54] Y. F. Niu, G. Colò, M. Brenna, P. F. Bortignon, and J. Meng, *Phys. Rev. C* **85**, 034314 (2012), URL <https://link.aps.org/doi/10.1103/PhysRevC.85.034314>.
- [55] M. Dutra, O. Lourenço, J. S. Sá Martins, A. Delfino, J. R. Stone, and P. D. Stevenson, *Phys. Rev. C* **85**, 035201 (2012), URL <https://link.aps.org/doi/10.1103/PhysRevC.85.035201>.

# SUPPLEMENTAL MATERIAL FOR “BAYESIAN INFERENCE OF THE LANDAU PARAMETER $G'_0$ FROM JOINT GAMOW-TELLER MEASUREMENTS”

## A. Definition of Landau parameters

We assume we have a spin-isospin zero-range interaction,

$$V_{\sigma\sigma\tau\tau} = V\delta(\vec{r}_1 - \vec{r}_2)\vec{\sigma}_1 \cdot \vec{\sigma}_2 \vec{\tau}_1 \cdot \vec{\tau}_2. \quad (\text{X.1})$$

The Skyrme p-h interaction that we employ in this work has this form, as detailed e.g. in Appendix F of [1]. To extract the Landau parameters  $G'_\ell$ , one writes the matrix elements of the interaction between plane waves,  $\langle \vec{k}_1 \vec{k}_2 | V_{\sigma\sigma\tau\tau} | \vec{k}_1 \vec{k}_2 \rangle$ . If we restrict to  $k_1 = k_2 = k_F$ , these matrix elements can only depend on the angle  $\theta$  between  $\vec{k}_1$  and  $\vec{k}_2$ , and are conventionally written, in the Landau-Migdal theory, as

$$\langle \vec{k}_1 \vec{k}_2 | V_{\sigma\sigma\tau\tau} | \vec{k}_1 \vec{k}_2 \rangle = N_0^{-1} \sum_{\ell} G'_\ell P_\ell(\cos\theta). \quad (\text{X.2})$$

The quantity  $N_0$  is the number of states around the Fermi surface per unit volume and unit energy, that is, in symmetric matter,

$$N_0 = \frac{2k_F m^*}{\pi^2 \hbar^2}. \quad (\text{X.3})$$

Then

$$N_0^{-1} = \frac{\pi^2 \hbar^2}{2k_F m^*} \approx 150 \text{ MeV} \cdot \text{fm}^3 \frac{m}{m^*}. \quad (\text{X.4})$$

As mentioned in various papers (Ref. [2] and p. 527 of [3]), there are different conventions (like e.g. using the density of states for a Fermi gas with two particles per momentum state: this would produce a value of  $N_0^{-1}$  that is a factor of two times larger, around  $\approx 300 \text{ MeV} \cdot \text{fm}^3$ . Notably, the Jülich group has used this convention.)

The groups working with a  $\pi + \rho$ -residual p-h force use a different convention for the Landau parameters because the quantity  $N_0^{-1} G'_0$  is replaced by  $\frac{f_\pi^2}{m_\pi^2} g'$ . We follow Ref. [2] in using a lowercase letter to indicate the Landau parameter written with this convention. The key quantity is

$$\frac{f_\pi^2}{m_\pi^2} \approx 392 \text{ MeV} \cdot \text{fm}^3. \quad (\text{X.5})$$

In [2], the notation  $4\pi f_\pi^2$  is used instead of  $f_\pi^2$ .

Then, the equivalence with the Landau parameter in the previous convention (uppercase letter) reads

$$N_0^{-1} G'_0 = G'_0 150 \text{ MeV} \cdot \text{fm}^3 \frac{m}{m^*} = \frac{f_\pi^2}{m_\pi^2} g'_0 = g'_0 392 \text{ MeV} \cdot \text{fm}^3. \quad (\text{X.6})$$

This is the same as Eq. (29) of [4], where only  $\hbar \equiv 1$ .

## B. The systematic model uncertainty in Bayesian inference

In state-of-the-art Bayesian inference, the systematic uncertainty of theoretical models is treated as an unknown property of the models. The “intrinsic scattering (IS) parameters” are applied in the Bayesian inference of this work as additional degrees of freedom. Here, the IS parameters of  $\hat{O}_k$  are defined as the logarithm of the ratio of systematic uncertainty to the mean of experimental measurement:

$$\text{IS} = \log_{10} \left( \frac{\sigma_{k,\text{sys}}}{O_{k,\text{mean}}} \right), \quad (\text{X.7})$$

where  $O_{k,\text{mean}}$  is the mean of experimental measurement, and  $\hat{O}_k$  is the theoretical prediction. In Fig. X.1, we present the posterior distribution of the intrinsic parameters. In this work, we have six intrinsic scattering parameters, which represent the systematic uncertainty of  $m_0\%$  in finite nuclei (black solid curve), the systematic uncertainty of the GTR peak location (blue



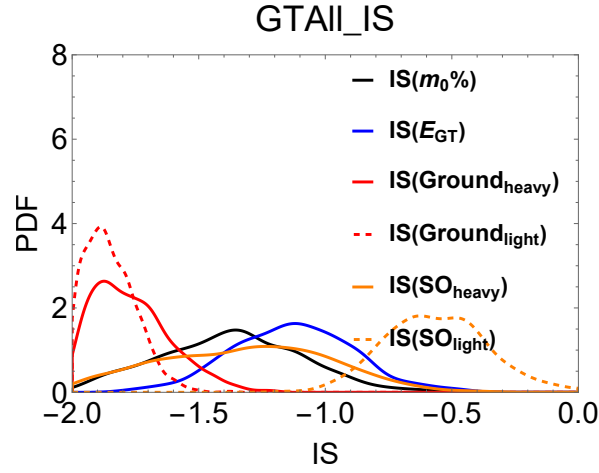


Figure X.1. The intrinsic scattering parameters in the GTAI Bayesian inference described in the text.

solid curve), the systematic uncertainty of heavy nuclei ground state properties (red solid curve), the systematic uncertainty of light nuclei ground state properties (red dashed curve), the systematic uncertainty of heavy nuclei spin-orbit splittings (orange solid curve) and the systematic uncertainty of light nuclei spin-orbit splittings (orange dashed curve). In this work, the ground state properties (the  $R_{ch}$  and  $E_{bind}$ ) and spin-orbit (SO) splitting properties of “heavy” nuclei include those of  $^{208}\text{Pb}$  and  $^{132}\text{Sn}$ . The ground-state properties and the SO properties of “light” nuclei involve those of  $^{90}\text{Zr}$  and  $^{48}\text{Ca}$ . We observe that the IS value of ground-state properties remains small, while the IS value of SO splitting (especially for those of light nuclei) becomes large, which suggests a potential tension between the fitting of SO splitting properties and the fitting of other finite nuclei properties within the Skyrme EDF ansatz.

### C. Bayesian Constraints

In table. X.1, we summarize the experimental constraints in the Bayesian inference with joint GTR measurements. The relative uncertainties of the experimental charge radii and binding energy are chosen as 2% to ensure the feasibility of Monte Carlo simulations. The mean values and uncertainty of the spin-orbit splitting are estimated based on the data summarized in [5]. In addition, the averaged values of the posterior properties of basic nuclei, spin-orbit splitting properties, and GT properties are listed in the table. By comparing them with experimental measurements, obvious tensions between theoretical and experimental measurements of spin-orbit splitting values of light nuclei and neutron skin thickness ( $\Delta F = F_{ch} - F_w$ ) of  $^{48}\text{Ca}$  and  $^{208}\text{Pb}$  are observed.

### D. The Bayesian Posterior

We first discuss the Bayesian posterior of ground state properties. In Fig. X.2, we present the ground-state properties ( $R_{ch}$ , BE,  $F_{ch}$  and  $\Delta F$ ) sampled from the posterior distribution of  $^{208}\text{Pb}$ ,  $^{132}\text{Sn}$ ,  $^{90}\text{Zr}$  and  $^{48}\text{Ca}$ . The posterior distributions are constrained by joint GTR measurements of  $^{208}\text{Pb}$ ,  $^{132}\text{Sn}$ ,  $^{90}\text{Zr}$ . The mean values of  $R_{ch}$ , BE,  $F_{ch}$  are close to the experimental measurements, and have a variation of approximately 5% with respect to the experimental values. In the lower right panel, the values of the form factor difference  $\Delta F = F_{ch} - F_w$  of  $^{208}\text{Pb}$  and  $^{48}\text{Ca}$  sampled from the posterior are represented by the scattered blue points. The form factor difference predicted by Skyrme models have a difficulty in simultaneously explaining the PREXII [9] and CREX [8] results, which is a known puzzle in the nuclear physics community. The letters “a”, “b” and “c” in the panels of Fig. X.2 represent the corresponding ground state values of nuSkyI, nuSkyII and nuSkyIII.

The Skyrme parameters of these three sets are summarized in the Tab. X.2. The nuSkyI has the highest total likelihood among a subset of the dataset sampled from the posterior distribution, where the mean of intrinsic scattering parameters (X.7)  $< -1.7$  (which corresponds to a systematic uncertainty  $< 2\%$ ). The nuSkyII has the highest total likelihood among the full dataset sampled from the posterior distribution. The nuSkyIII has the highest total likelihood among a subset of the dataset where the parameterizations have reasonable infinite dense matter bulk properties from low to high densities so that they can be used to describe neutron star properties. This subset is defined by requiring that 1) the effective mass of protons and neutrons

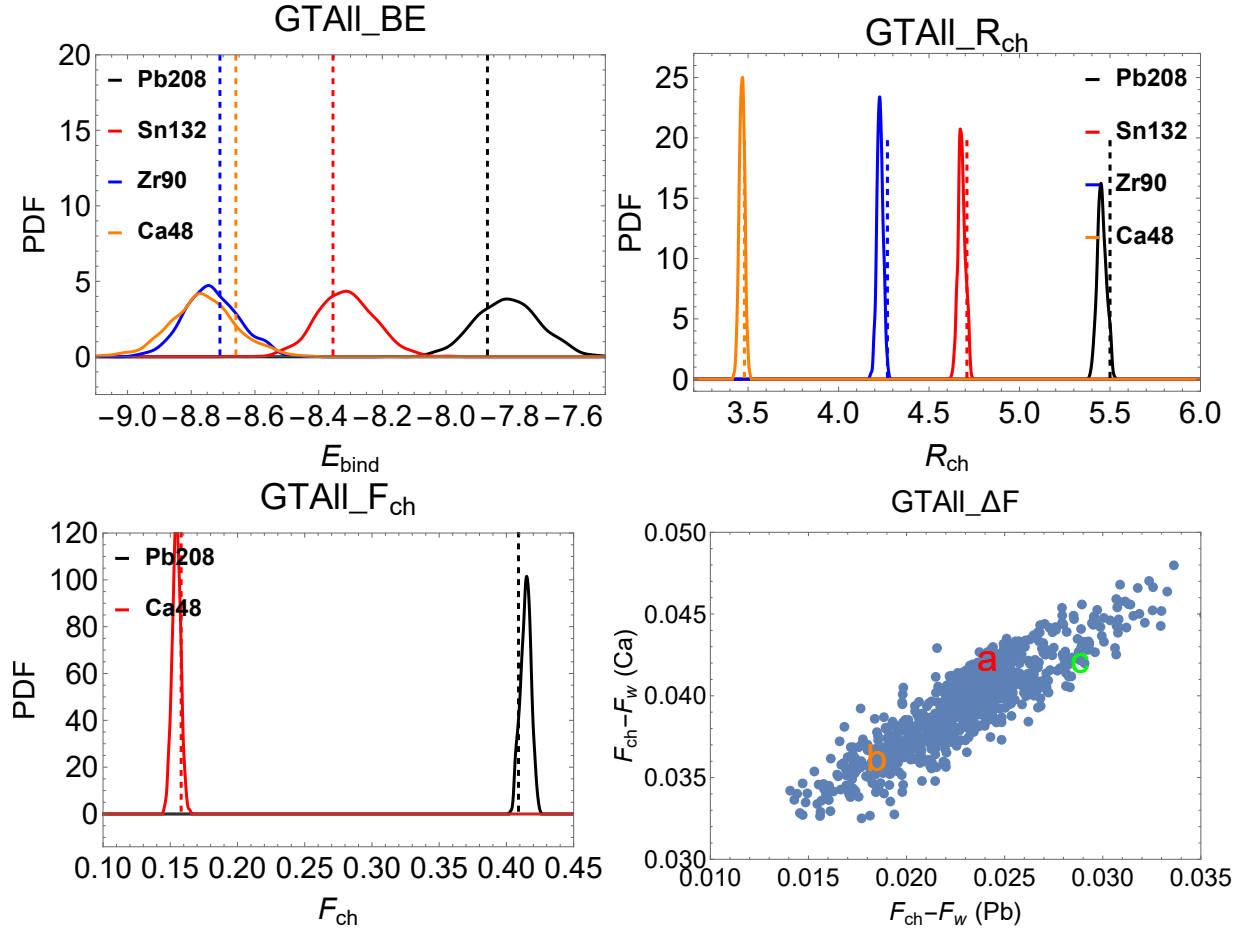


Figure X.2. The ground state properties of the Skyrme parameterizations, sampled from the GTAIL calculations described in the text. In the upper left panel, we present the binding energy of  $^{208}\text{Pb}$ ,  $^{132}\text{Sn}$ ,  $^{90}\text{Zr}$  and  $^{48}\text{Ca}$  sampled from the posterior distribution. In the upper right panel, we present the charge radii of  $^{208}\text{Pb}$ ,  $^{132}\text{Sn}$ ,  $^{90}\text{Zr}$  and  $^{48}\text{Ca}$  sampled from the posterior distribution. In the lower left panel, we present the charge form factor of  $^{208}\text{Pb}$  and  $^{48}\text{Ca}$  sampled from the posterior distribution and in the lower right panel we present the  $F_{ch} - F_w$  of  $^{208}\text{Pb}$  and  $^{48}\text{Ca}$  sampled from the posterior distribution. The letters “a”, “b” and “c” represent the corresponding ground state values from nuSkyI, nuSkyII and nuSkyIII, respectively.

up to several times saturation density is positive; 2) the speed of sound up to several times saturation density is positive; 3) the beta equilibrium can be achieved up to several times saturation density; 4) the di-neutron state does not appear below saturation density by requiring that the energy per nucleon is always positive in pure neutron matter.

The Skyrme parameters  $b_4$  and  $b'_4$  have obvious influence on spin-orbit splitting and GT properties in finite nuclei. In Fig. X.3, we present the posterior of  $b_4$  and  $b'_4$  in two Bayesian inferences: one based on noGT (dashed curves) and one based on GTAIL (solid curves). The inclusion of GTR constraints significantly change the distribution of these two Bayesian parameters. The posterior of the latter suggests that  $b'_4 > b_4 > 0$ . The unit of  $b'$  and  $b'_4$  presented in the figure is  $\text{fm}^4$ , rather than  $\text{MeV fm}^5$ .

In Fig. X.4, we present the spin-orbit splitting properties of  $^{208}\text{Pb}$ ,  $^{90}\text{Zr}$  and  $^{48}\text{Ca}$  sampled from the posterior distribution with GTR constraints from  $^{208}\text{Pb}$ ,  $^{132}\text{Sn}$ ,  $^{90}\text{Zr}$ . The neutron SO splittings of  $^{208}\text{Pb}$  investigated in this work are  $\nu 1i_{13/2}^{-1} - \nu 1i_{11/2}$  ( $\nu 1i$  in the figure),  $\nu 3p_{3/2}^{-1} - \nu 3p_{1/2}$  ( $\nu 3p$  in the figure),  $\nu 2f_{7/2}^{-1} - \nu 2f_{5/2}$  ( $\nu 2f$  in the figure). The proton SO splittings of  $^{208}\text{Pb}$  investigated in this work are  $\pi 2f_{7/2} - \pi 2f_{5/2}$  ( $\pi 2f$  in the figure),  $\pi 3p_{3/2} - \pi 3p_{1/2}$  ( $\nu 3p$  in the figure). The neutron SO splittings of  $^{90}\text{Zr}$  investigated in this work are  $\nu 1g_{9/2}^{-1} - \nu 1g_{7/2}$  ( $\nu 1g$  in the figure). The proton SO splittings of  $^{90}\text{Zr}$  investigated in this work are  $\pi 1g_{9/2} - \pi 1g_{7/2}$  ( $\pi 1g$  in the figure). The neutron SO splittings of  $^{48}\text{Ca}$  investigated in this work are  $\nu 1f_{7/2}^{-1} - \nu 1f_{5/2}$  ( $\nu 1f$  in the figure). The proton SO splittings of  $^{48}\text{Ca}$  investigated in this work are  $\pi 1f_{7/2} - \pi 1f_{5/2}$  ( $\pi 1f$  in the figure). Our models reasonably predict SO splittings in  $^{208}\text{Pb}$ , but have difficulties simultaneously explaining SO splittings in  $^{90}\text{Zr}$  and  $^{48}\text{Ca}$ , resulting in the large IS parameters discussed in Section B. The experimental SO splitting values are represented by the dashed vertical line, which is the mean value reported in Table III of [5]. The letters “a”, “b” and “c” represent the corresponding SO splitting values from nuSkyI, nuSkyII and nuSkyIII.

	Property	Experiment	Error	Mean of Posterior
Bulk properties of nuclei [6, 7]	$R_{ch}^{48Ca}$ [fm]	3.48	0.069	3.47
	$R_{ch}^{90Zr}$ [fm]	4.27	0.085	4.23
	$R_{ch}^{132Sn}$ [fm]	4.71	0.09	4.68
	$R_{ch}^{208Pb}$ [fm]	5.50	0.11	5.46
	$BE^{48Ca}$ [MeV]	8.67	0.17	8.76
	$BE^{90Zr}$ [MeV]	8.71	0.17	8.73
	$BE^{132Sn}$ [MeV]	8.355	0.17	8.31
	$BE^{208Pb}$ [MeV]	7.87	0.16	7.80
CREX	$F_{ch}^{48Ca} - F_w^{48Ca}$ []	0.0277	0.0055	0.039
PREX [8, 9]	$F_{ch}^{208Pb} - F_w^{208Pb}$ []	0.041	0.013	0.0229
Spin-orbit splitting constraints [5]	$\nu 1f_{7/2}^{-1} - \nu 1f_{5/2}^{-1}$ ( $^{48}\text{Ca}$ ) [MeV]	8.41	0.67	6.14
	$\pi 1f_{7/2}^{-1} - \pi 1f_{5/2}^{-1}$ ( $^{48}\text{Ca}$ ) [MeV]	4.92	0.39	6.70
	$\nu 1g_{9/2}^{-1} - \nu 1g_{7/2}^{-1}$ ( $^{90}\text{Zr}$ ) [MeV]	7.07	0.57	6.01
	$\pi 1g_{9/2}^{-1} - \pi 1g_{7/2}^{-1}$ ( $^{90}\text{Zr}$ ) [MeV]	5.56	0.44	6.52
	$\nu 1i_{13/2}^{-1} - \nu 1i_{11/2}^{-1}$ ( $^{208}\text{Pb}$ ) [MeV]	5.91	0.42	5.82
	$\nu 3p_{3/2}^{-1} - \nu 3p_{1/2}^{-1}$ ( $^{208}\text{Pb}$ ) [MeV]	0.90	0.052	0.89
	$\nu 2f_{7/2}^{-1} - \nu 2f_{5/2}^{-1}$ ( $^{208}\text{Pb}$ ) [MeV]	2.06	0.12	2.36
	$\pi 2f_{7/2}^{-1} - \pi 2f_{5/2}^{-1}$ ( $^{208}\text{Pb}$ ) [MeV]	1.96	0.053	1.92
Gamow-Teller constraints	$\pi 3p_{3/2}^{-1} - \pi 3p_{1/2}^{-1}$ ( $^{208}\text{Pb}$ ) [MeV]	0.607	0.21	0.69
	$E_{GT}$ ( $^{90}\text{Zr}$ )	15.8	0.32	15.82
	$E_{GT}$ ( $^{132}\text{Sn}$ )	13.97	0.28	13.97
	$E_{GT}$ ( $^{208}\text{Pb}$ )	19.2	0.38	19.36
	$m_0\%$ ( $^{90}\text{Zr}$ )	68%	1.4%	72.0%
	$m_0\%$ ( $^{132}\text{Sn}$ )	81.0%	16%	79.23%
	$m_0\%$ ( $^{208}\text{Pb}$ )	74%	1.48%	76.0%

Table X.1. The full list of experimental constraints applied in the Bayesian inference of this work.

Skyrme Parameter	nuSkyI	nuSkyII	nuSkyIII
$t_0$ [MeV fm <sup>3</sup> ]	-2585.9	-2896.91	-2604.99
$t_1$ [MeV fm <sup>5</sup> ]	509.532	508.693	538.016
$t_2$ [MeV fm <sup>5</sup> ]	-68.789	35.414	25.3424
$t_3$ [MeV fm <sup>3+3<math>\alpha</math>]</sup>	13071.1	15233.2	13238.5
$x_0$ []	0.456306	0.296407	0.176233
$x_1$ []	-0.259363	0.617636	-0.212738
$x_2$ []	-0.579601	-3.79921	-4.40879
$x_3$ []	0.732344	0.207303	0.200248
$\alpha$ []	0.129909	0.115935	0.13045
$b_4$ [fm <sup>4</sup> ]	0.261995	0.133732	0.161697
$b'_4$ [fm <sup>4</sup> ]	0.270569	0.407115	0.524227

Table X.2. The Skyrme parameters of nuSkyI, nuSkyII and nuSkyIII.

We then discuss the posterior distributions of excited state properties. In Fig. X.5, we present the  $E_{GT}$  of  $^{208}\text{Pb}$ ,  $^{132}\text{Sn}$ ,  $^{90}\text{Zr}$  and  $^{48}\text{Ca}$  sampled from the posterior distribution with GTR constraints from  $^{208}\text{Pb}$ ,  $^{132}\text{Sn}$ ,  $^{90}\text{Zr}$ . The mean values of the posterior distribution of  $E_{GT}$  of  $^{208}\text{Pb}$ ,  $^{132}\text{Sn}$ ,  $^{90}\text{Zr}$  are close to the experimental measurements. In particular, the mean value of the posterior distribution of  $^{48}\text{Ca}$  is also close to the experimental measurement, demonstrating the predictive power of our Skyrme QRPA model. The letters “a”, “b” and “c” represent the corresponding  $E_{GT}$  values from nuSkyI, nuSkyII and nuSkyIII. The vertical positions of the letters are slightly tuned for readability.

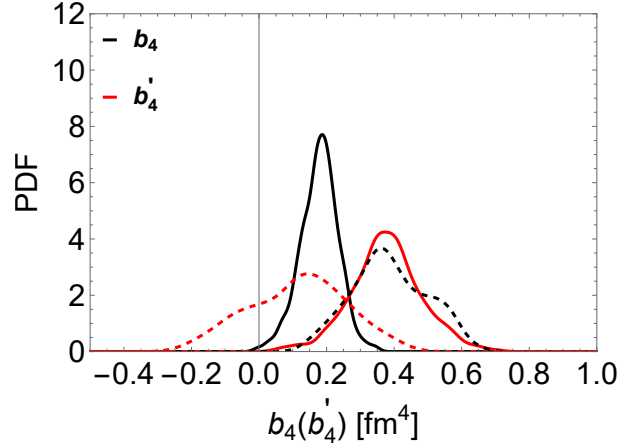


Figure X.3. The PDF of  $b_4$ ,  $b'_4$  sampled from GTAll Bayesian inference (solid curves) and noGT inference (dashed curves).

In Fig. X.6, we present the Pearson correlation coefficients among the GT quantities ( $m_0\%$  and  $E_{GT}$ ), the spin-orbit splitting values, and the ground state quantities from various nuclei. In the top (bottom) panel, the Pearson correlation coefficients are calculated based on posterior without (with) joint GTR constraints. The strength of Pearson correlations may or may not be sensitive to the Bayesian constraints. By comparing the top and bottom panel, we find interesting correlations insensitive to GTR constraints: 1) the  $m_0\%$  and  $E_{GT}$  of  $^{208}\text{Pb}$  (denoted as  $m_0^{\text{Pb}}\%$  and  $E_{GT}^{\text{Pb}}$ ) is strongly correlated with the  $m_0\%$  and  $E_{GT}$  of  $^{132}\text{Sn}$ ; 2) the  $E_{GT}$  of  $^{90}\text{Zr}$  is strongly correlated with the  $E_{GT}$  of  $^{48}\text{Ca}$ ; 3) the spin-orbit splitting of neutrons in the  $3p$  channel is strongly correlated with that of neutrons in the  $2f$  channel in  $^{208}\text{Pb}$  (denoted as  $\nu_{3p}^{\text{Pb}}$  and  $\nu_{2f}^{\text{Pb}}$ ); 4) the spin-orbit splitting of protons in the  $3p$  channel is strongly correlated with that of protons in the  $2f$  channel in  $^{208}\text{Pb}$  (denoted as  $\pi_{3p}^{\text{Pb}}$  and  $\pi_{2f}^{\text{Pb}}$ ); 5) the spin-orbit splitting values of  $^{48}\text{Ca}$  and  $^{90}\text{Zr}$  are strongly correlated; 6) the ground state properties (e.g. binding energy, charge radii) of heavy nuclei are strongly correlated; 7) the ground state properties of light nuclei are strongly correlated; 7) the ground state properties of heavy nuclei are correlated with those of light nuclei, but with less correlation strength. These obvious correlations appear as diagonal blocks in the figure.

We also observe correlations sensitive to GTR constraints: 1) the correlation between  $m_0\%$  and  $G'_0$  is more obvious in simulations without GTR constraints, which can be easily understood. In the Bayesian inference constrained by GTR measurements the  $m_0\%$  is severely restricted, resulting in the weakening of the correlation. In fact, if  $m_0\%$  is totally fixed, then no correlation involving  $m_0\%$  can be found; 2) the spin-orbit splitting values are correlated with the Skyrme parameters  $b_4$  and  $b'_4$ . These correlations are subtle and more obvious in simulations with joint GTR constraints. More studies are needed to confirm these correlations.

### E. Many-body correction on neutrino-nucleon reactions

Here, we introduce the basic formulas for calculating the many-body correction on charged current neutrino-nucleon reactions based on RPA. Based on linear response theory, the structure factor of neutrino-nucleon reactions is estimated as:

$$S(q_0, q) = \frac{2\text{Im}\Pi}{1 - \exp(-z)}, \quad (\text{X.8})$$

where  $z = q_0 + \mu_n - \mu_p$  for the reaction  $\nu_e + n \rightarrow p + e^-$ .

In frequency space, the polarization function  $\Pi$  is:

$$\Pi = 2 \int \frac{d^3k_2}{(2\pi)^3} G(q_0, q, \vec{k}_2), \quad (\text{X.9})$$

where  $G(q_0, q, \vec{k}_2)$  is a particle-hole propagator that obeys the Bethe-Salpeter equation:

$$\begin{aligned} G_{RPA}^\alpha(q_0, q, \vec{k}_1) &= G_{HF}(q_0, q, \vec{k}_1) + G_{HF}(q_0, q, \vec{k}_1) \\ &\times \sum_{\alpha'} \int \frac{d^3k_2}{(2\pi)^3} V_{ph}^{\alpha, \alpha'}(q, \vec{k}_1, \vec{k}_2) \times G_{RPA}^{\alpha'}(q_0, q, \vec{k}_2), \end{aligned} \quad (\text{X.10})$$

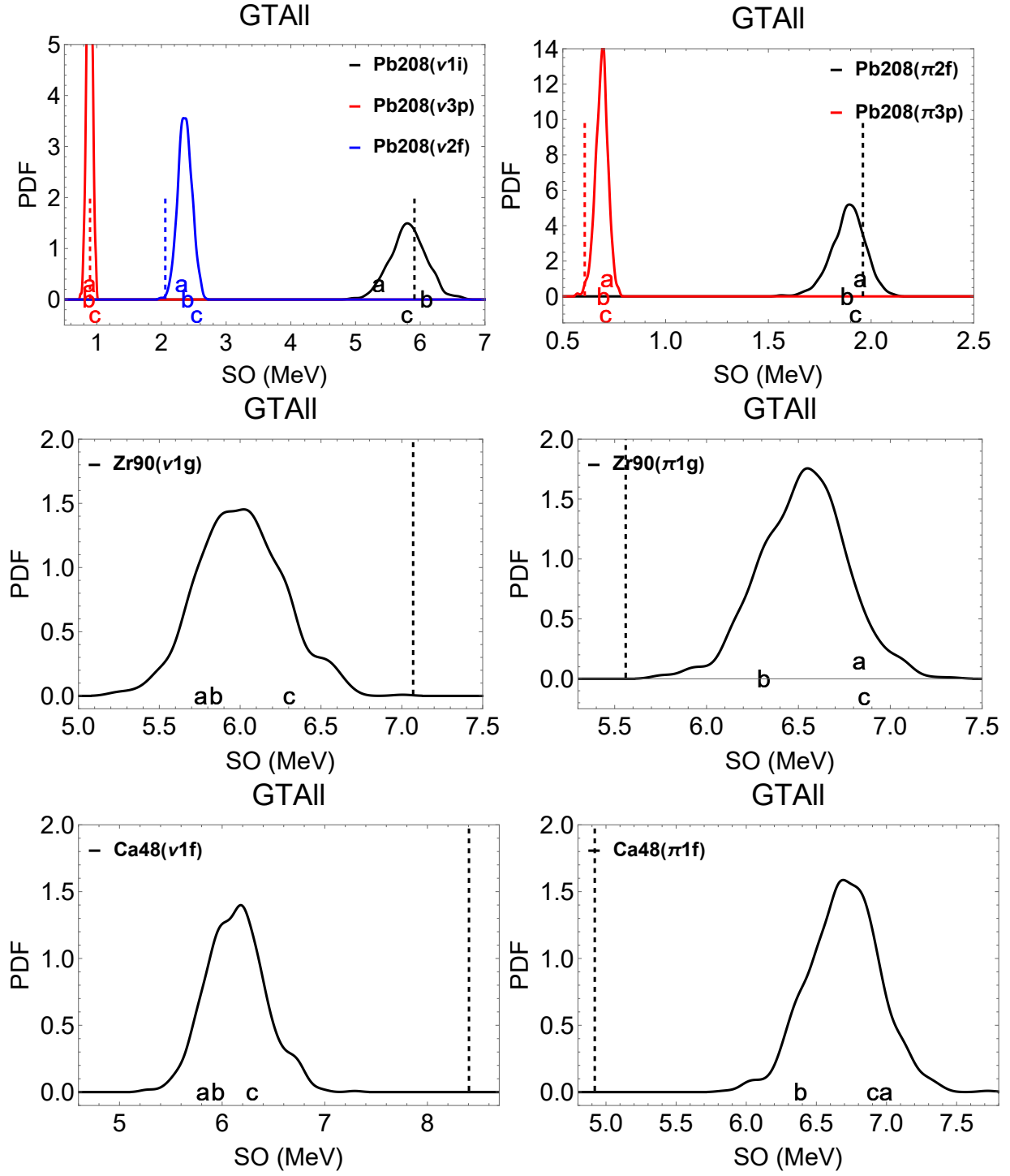


Figure X.4. The excited state properties of the Skyrme parameterizations based on GTaII calculations. In the upper left (right) panel, we present the neutron (proton) spin-orbit splittings of  $^{208}\text{Pb}$  sampled from the posterior distribution. In the middle left (right) panel, we present the neutron (proton) spin-orbit splitting of  $^{90}\text{Zr}$  sampled from the posterior distribution. In the lower left (right) panel, we present the neutron (proton) spin-orbit splitting of  $^{48}\text{Ca}$  sampled from the posterior distribution. The letter “a”, “b” and “c” represent the corresponding ground state values from nuSkyI, nuSkyII and nuSkyIII, respectively. The vertical positions of the letters are slightly tuned for readability.

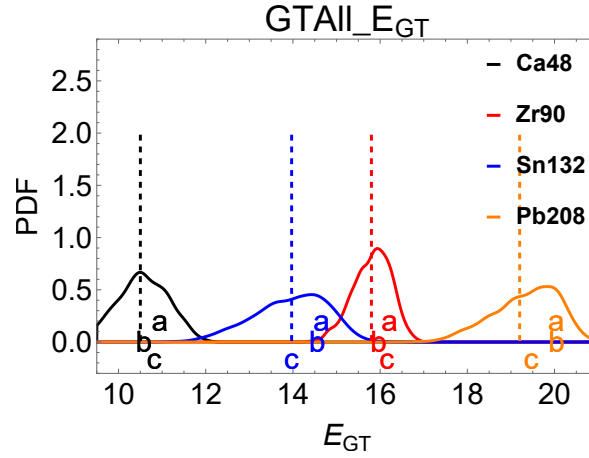


Figure X.5. The  $E_{GT}$  of  $^{208}\text{Pb}$ ,  $^{132}\text{Sn}$ ,  $^{90}\text{Zr}$  and  $^{48}\text{Ca}$  sampled from the GTail calculations. The letter “a”, “b” and “c” represent the corresponding ground state values from nuSkyI, nuSkyII and nuSkyIII, respectively. The vertical positions of the letters are slightly tuned for readability.

with  $\alpha = 0$  (1) representing non-spin-flip (spin-flip) channels and  $V_{ph}^{\alpha,\alpha'} = \delta(\alpha - \alpha')[W_1^\alpha(q) + W_2^\alpha(q)(\vec{k}_1 - \vec{k}_2)^2]$ . The  $W_{1,2}^\alpha$  functions are functions of Skyrme parameters and are summarized in [10, 11]. The  $G_{HF}$  is defined as

$$G_{HF} = \frac{n_n(\vec{k}) - n_p(\vec{k} + \vec{q})}{q_0 - (E_p(\vec{k} + \vec{q}) - E_n(\vec{k})) + i\eta}. \quad (\text{X.11})$$

To solve the Bethe-Salpeter equation, we follow the strategy proposed in [10, 12]. By integrating both the right- and left-hand sides of the equation (X.10) over  $\vec{k}_1$  and expanding in multipoles the residual interaction  $V_{ph}$ , the Bethe-Salpeter equation can be re-written as a system of algebraic equations, from which the  $\langle G \rangle_{RPA} = \Pi/2$  can be solved for:

$$\begin{aligned} \langle G \rangle_{RPA} = & (\beta_0 + 2W_2^\alpha(\beta_0\beta_3 - \beta_1^2)q^2) \\ & / \{1 - W_1^\alpha\beta_0 + 2q^2W_2^\alpha[-\beta_2 + \beta_3 + W_1^\alpha(\beta_1^2 - \beta_0\beta_3)] + q^4(W_2^\alpha)^2[-\beta_0\beta_5 + 4(\beta_1\beta_4 - \beta_2\beta_3) + \beta_2^2] \\ & + 2q^6(W_2^\alpha)^3[-\beta_0\beta_3\beta_5 + \beta_0\beta_4^2 + \beta_1^2\beta_5 - 2\beta_1\beta_2\beta_4 + \beta_2^2\beta_3]\}, \end{aligned} \quad (\text{X.12})$$

where  $W_i^\alpha$  are given by Eq. (7-10) of [10],  $\beta_l = \int \frac{d^3k}{(2\pi)^3} G_{HF} F_l$ ,  $\langle G \rangle_{RPA} = \int \frac{d^3k}{(2\pi)^3} G_{RPA}$  and

$$F_{0-5} = \{1, \frac{\vec{k} \cdot \vec{q}}{q^2}, \frac{k^2}{q^2}, \frac{(\vec{k} \cdot \vec{q})^2}{q^4}, \frac{\vec{k} \cdot \vec{q} k^2}{q^4}, \frac{k^4}{q^4}\}, \quad (\text{X.13})$$

Given the  $\langle G \rangle_{RPA}$ , we then obtained the dynamic structure factor of  $S(q_0, q)$  by using eq. (X.8). Interested readers are referred to [10, 11, 13] for detailed calculation of the many-body correction on neutrino opacities in CCSNe and BNS mergers.

The dispersion relation of nucleons follows  $E_N(\vec{k}) = \frac{k^2}{2m^*} + U_N$ . Consequently, the in-medium nucleon potential difference  $\delta U = U_n - U_p$  heavily influences the Hartree-Fock propagator  $G_{HF}$ , the  $G_{RPA}$  and the  $S(q_0, q)$ .

## F. The extraction of $G'_0$

In this section, we choose a Skyrme parameterization (SAMI [14]) as fiducial model, to test the robustness of the extraction methodology of  $G'_0$  suggested by [15]. In [15],  $G'_0$  is obtained from the GTR energy in the mother nucleus as

$$E_{GTS} - E_d = \epsilon_d + \frac{2}{3T_0} \Delta E(l\sigma) + 4\kappa_{\sigma\tau} T_0, \quad (\text{X.14})$$

where  $\epsilon_d$  is the average unperturbed excitation energy,  $\Delta E(l\sigma)$  is the average spin-orbit splitting value, and  $T_0 = (N - Z)/2$ . The  $\kappa_{\sigma\tau}$  is proportional to the Landau-Migdal parameter  $G'_0$ :

$$A\kappa_{\sigma\tau} = G'_0 \frac{k_F^2}{3m^*} \gamma, \quad (\text{X.15})$$

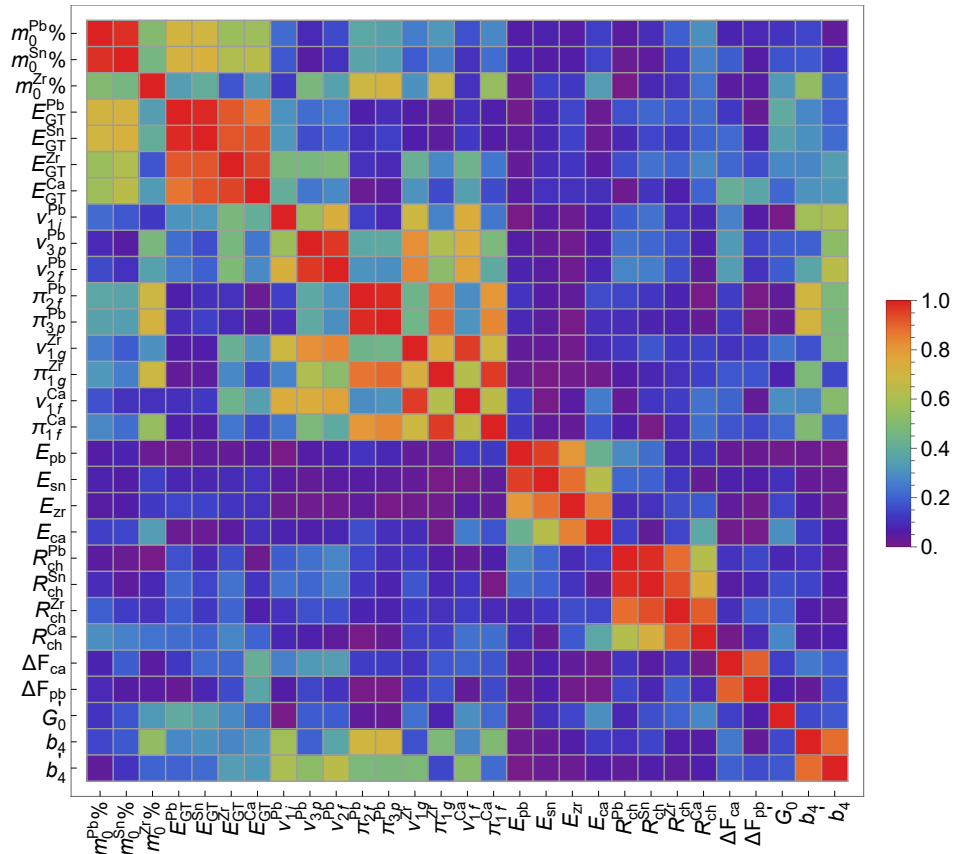


Figure X.6. The Pearson correlation coefficients among the Gamow-Teller excited state features (e.g.  $m_0\%$ ,  $E_{\text{GT}}$ ) and ground state features on various nuclei. The top (bottom) panel represents the correlations of the sampled data from the noGT (GTall) calculations described in the text. The top (bottom) panel does not include (includes) the Gamow-Teller constraints.

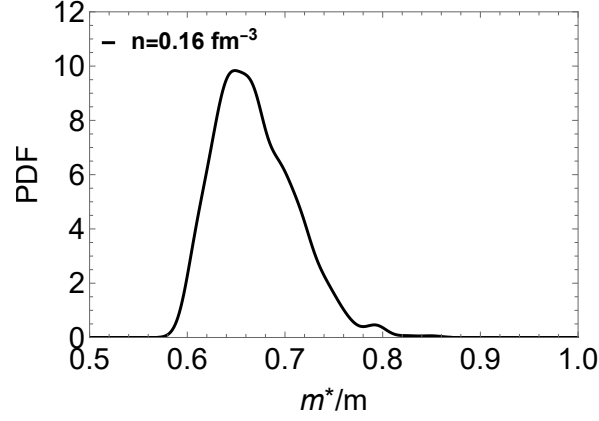


Figure X.7. The probability density distribution of  $m^*/m$  in symmetric nuclear matter at  $n = 0.16 \text{ fm}^{-3}$ , inferred by the GTAll calculations described in the text. The mean of  $m^*/m$  is 0.67.

where  $A$  is the total nucleon number,  $k_F = 1.36 \text{ fm}^{-1}$ ,  $m^*$  is the effective mass and  $\gamma$  is roughly approximated as 0.5 in [15].

We use the prediction of  $E_{\text{GT}}$ ,  $\epsilon_d$ , and  $\Delta E(l\sigma)$  by SAMI to deduce  $G'_0$  following Eq. (X.15). The deduced value is expected to be close to  $G'_0$  of the SAMi model. For  $^{208}\text{Pb}$ , SAMi predicts that  $E_{\text{GTS}} - E_\pi = 19.2 \text{ MeV}$  (which corresponds to  $E_{\text{GTS}} - E_d = 15.54 \text{ MeV}$ ),  $\epsilon_d = 7.52 \text{ MeV}$ ,  $\Delta E(l\sigma) = 2.47 \text{ MeV}$  and  $m^*/m = 0.66$ , which in turn gives  $G'_0 \approx 0.69$ . However, the exact  $G'_0$  corresponding to the SAMi interaction is 0.35, which is about one-half of the value extracted using Eq. X.15. This suggests that the larger  $G'_0$  extracted from traditional empirical models may result from the fact that these models used simplified assumptions (e.g., density-independent  $G'_0$  and, in the case of [15], a schematic solution of RPA as well as a constant attenuation factor  $\gamma$ ). Additionally, empirical models do not self-consistently calculate the effective nucleon mass, and an approximation of  $0.8 \lesssim m^*/m \lesssim 1.0$  is usually used. However, as shown in Fig. X.7, the effective masses sampled from our Bayesian inference (where the mean of  $m^*/m$  is 0.67) indicate that the effective mass may very likely be smaller than the former assumptions, which induces large  $G'_0$  in previous empirical works. A self-consistent model may be necessary to extract the Landau-Migdal parameter of infinite symmetric nuclear matter from the experimental measurements on finite nuclei.

- 
- [1] M. Bender, J. Dobaczewski, J. Engel, and W. Nazarewicz, Phys. Rev. C **65**, 054322 (2002), nucl-th/0112056.
  - [2] I. S. Towner, Phys. Rept. **155**, 263 (1987).
  - [3] F. Osterfeld, Rev. Mod. Phys. **64**, 491 (1992).
  - [4] T. Suzuki and M. Honma, Phys. Rev. C **87**, 014607 (2013), 1211.4078.
  - [5] M. Zalewski, J. Dobaczewski, W. Satula, and T. R. Werner, Phys. Rev. C **77**, 024316 (2008), 0801.0924.
  - [6] M. Wang, G. Audi, A. H. Wapstra, F. G. Kondev, M. MacCormick, X. Xu, and B. Pfeiffer, Chin. Phys. C **36**, 1603 (2012).
  - [7] I. Angeli and K. P. Marinova, Atom. Data Nucl. Data Tabl. **99**, 69 (2013).
  - [8] D. Adhikari et al. (CREX), Phys. Rev. Lett. **129**, 042501 (2022), 2205.11593.
  - [9] D. Adhikari et al. (PREX), Phys. Rev. Lett. **126**, 172502 (2021), 2102.10767.
  - [10] E. S. Hernandez, J. Navarro, and A. Polls, Nucl. Phys. A **658**, 327 (1999).
  - [11] Z. Lin, A. W. Steiner, and J. Margueron, Phys. Rev. C **107**, 015804 (2023), URL <https://link.aps.org/doi/10.1103/PhysRevC.107.015804>.
  - [12] J. Margueron, J. Navarro, and N. Van Giai, Phys. Rev. C **74**, 015805 (2006), nucl-th/0604019.
  - [13] S. Reddy, M. Prakash, J. M. Lattimer, and J. A. Pons, Phys. Rev. C **59**, 2888 (1999), URL <https://link.aps.org/doi/10.1103/PhysRevC.59.2888>.
  - [14] X. Roca-Maza, G. Colo, and H. Sagawa, Phys. Rev. C **86**, 031306 (2012), 1205.3958.
  - [15] T. Suzuki, Nucl. Phys. A **379**, 110 (1982).